First-principles method for the phonon-limited resistivity of metals

Tue Gunst*, Anders Blom‡ and Kurt Stokbro†
* DTU Nanotech, Center for Nanostructured Graphene (CNG), Technical University of Denmark, Denmark
Email: Tue.Gunst@nanotech.dtu.dk
†Synopsys QuantumWise, Fruebjergvej 3, Postbox 4, DK-2100 Copenhagen, Denmark.
‡Synopsys, Inc., 690 E Middlefield Rd, Mountain View, CA 94043, USA.

***Abstract*—We present several extensions to the Boltzmann Transport Equation (BTE) solver implemented in QuantumATK. This enables computational efficient simulations of first-principles transport coefficients in linear response to an applied electric field, magnetic field or temperature gradient. We calculate the phonon-limited resistivity in three FCC metals (Gold, Silver and Cobber) with the calculation of scattering rates from the electron-phonon interaction from first-principles. We correctly find that Gold has the highest resistivity while the resitivity of Copper is only slightly larger than that of Silver. In addition, we find that the resistivity of a 1 nm diameter Au nanowire is more than doubled as compared to that of bulk Au due to the increased electron-phonon coupling in nanowires. The simulations illustrate the predictive capabilities of the implemented Boltzmann Transport Equation (BTE) solver.**

I. Introduction

The continued downscaling of nanoelectronics makes the metal interconnects an increasingly important part of transistors[1]. Size-dependent phenomena as well as the detailed atomic structure may be considered as limiting factors in future devices. Present day transistors use copper as an interconnect material. Recently, industrial key players have shown a fundamental interest in understanding the dramatic increase in resistance observed in Cu nanowires compared to the bulk material[2]. Understanding the origin of this resistance increase will be important for the design and performance of future nanoscale devices and might vary on the metallic compound used in the interconnect. Size-dependent phenomena as well as an increased coupling between current and atomic vibrations (electron-phonon coupling) will play an important role in such devices[3], [4]. First-principles simulations may play a key role in understanding the mechanisms behind and find replacement materials for future interconnects. Using Density Functional Theory (DFT) simulations is an attractive approach, since it can accurately describe the atomic-scale details and electronic structure of surfaces, interfaces and different material combinations without the use of any experimental data[5].

In this paper, we calculate the first-principles phonon-limited resistivity with the QuantumATK[6] simulation tool and Boltzmann solver[7] of three different FCC metals typically used in interconnects. We present the extension of the Boltzmann solver with a tetrahedron integrations scheme, tensor analysis and an energy-dependent (**k**-space isotropic) scattering rate. The tetrahedron integration scheme is especially important for metals due to the extended Fermi surface, and we discuss the overall strategies to efficient Boltzmann transport simulations for either semiconductors or metals.

II. Theory

First-principles simulations of the resistivity is rather demanding as one need to integrate the coupling over both electron and phonon wavevectors (k- and q-space) and only few studies of electron-phonon coupling in metals exist[8], [9]. We have developed a fast and reliable simulation tool that enable efficient computations of the phonon-limited resistivity of metals using several approaches different from those used in semiconductors. Next we will describe the linear response transport formalism implemented. Then we will discuss how a clever selection of k- and q-points can be applied in semiconductors, see example in Fig.1a, while for metals we have found it more efficient to perform tetrahedron integration over the entire Brillouin zone (BZ) due to the extended Fermi-surface, Fig.1b. Combining either direct integrations for semiconductors and semimetals or tetrahedron integrations for metals gives an efficient and tractable simulation tool for phonon-limited mobilities of materials.

A. Transport coefficients

QuantumATK can calculate linear response coefficients related to the application of an electric field, temperature gradient or magnetic field in bulk materials. The current density is expanded to lowest order in the electric field $\mathcal{E}$, magnetic field B, and temperature difference ∇T:

$$\mathbf{j} = \sigma_{ij}\mathcal{E}_j + \sigma_{ijl}\mathcal{E}_j B_l + \nu_{ij}\nabla_j T \tag{1}$$

where the indices label Cartesian directions and σ_{ij}, σ_{ijk} and ν_{ij} are the electronic conductivity, Hall conductivity and thermoelectric response. Following the expressions in Ref. [10], the band-dependent thermoelectric transport coefficients and Hall coefficients can be obtained as

$$\begin{aligned}\sigma_{ij}(n\mathbf{k}) &= e^2\tau(n\mathbf{k})\mathbf{v}_i(n\mathbf{k})\mathbf{v}_j(n\mathbf{k})\,,\\ \sigma_{ijl}(n\mathbf{k}) &= e^3\tau^2(n\mathbf{k})\varepsilon_{luv}\mathbf{v}_i(n\mathbf{k})\mathbf{v}_v(n\mathbf{k})\mathbf{M}^{-1}_{ju}(n\mathbf{k})\end{aligned} \tag{2}$$

where ε_{kuv} is the Levi-Civita symbol. The band group velocities $\mathbf{v}(nk)$ and effective mass tensors $\mathbf{M}^{-1}(n\mathbf{k})$ are obtained through perturbation theory. In QuantumATK we have the

978-1-5386-6790-3/18/$31.00 ©2018 IEEE

option to include the full scattering rate, $\tau(n\mathbf{k})$, obtained from first-principles electron-phonon coupling or another energy or k-space dependent scattering rate to go beyond the constant scattering rate approximation used in Ref. [10]. In the following, we will describe the calculation of the first-principles scattering rate from electron-phonon coupling and present results for bulk metals and nanowires.

B. Bulk mobility

Next we will explain the steps taken towards efficient and tractable mobility calculations in QuantumATK. Previously, the implementation in QuantumATK performed the k-space and q-space integrations by direct summations over samplings of the relevant minimal areas in momentum-space [7]. This is highly efficient if the relevant q-points are limited in space and easy to define. We will now discuss when this is the case and an alternative option used in the case of metals.

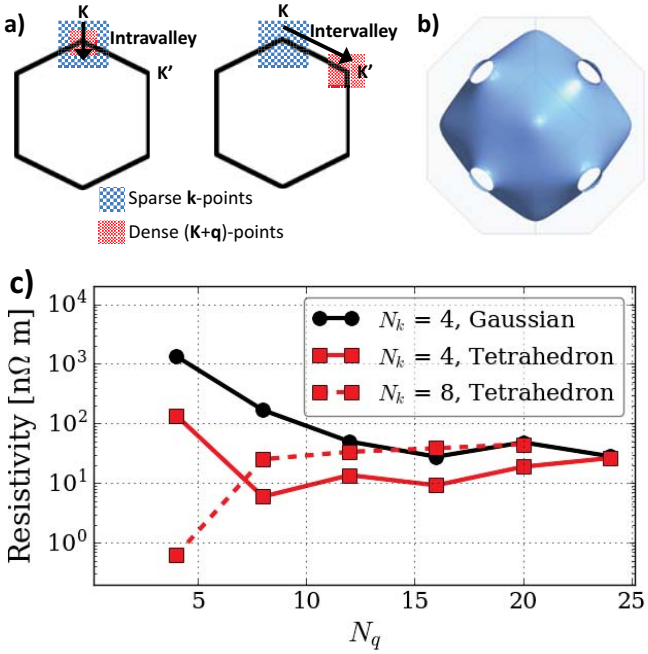

Fig. 1. (a) Illustrative k- and q-point selections in the Brillouin zone in the case of a two-dimensional semiconductor with two valleys (K and K'). In semiconductors it is possible to make a clever selection of k-points and q-points to minimize the computational burden while including all relevant scattering processes. Typically a sparse k-point sampling is used for the mobility integral while a denser q-point sampling is needed to secure a correct scattering rate at each k-point. (b) Fermi-surface of bulk Au. In metals k-points contributing to the neighborhood of the Fermi-surface are not located in a small subset of the Brillouin zone. Therefore k- and q-points are sampled in the full Brillouin zone and q-space integrated by a tetrahedron method to minimize the sampling density. (c) Convergence with respect to the number of q-points for bulk Au with either a direct or tetrahedron integration over the full Brillouin zone.

Typically the relevant k-points are found by searching for k-points where the bandstructure has energies in a specific range chosen to be consistent with wanted Fermi-level shifts or corresponding charge carrier densities. Alternatively, this is done internally in the software by specifying an energy range for the initial state.

In semiconductors or semi-metals the q-points can in many materials be chosen in a clever manner to sample the relevant intra- and inter-valley scatterings. This holds for two-dimensional materials like graphene and MoS_2 where intra-valley scattering is obtained by selecting k-points near the Dirac point and sampling q-points in a region around the Γ-point, Fig.1a. Inter-valley scattering is then obtained by sampling q-points connecting the two Dirac points (E.g. the intra-valley points plus the distance between the valleys). Correspondingly, for Silicon one select k-points in one valley and q-points either around the Γ-point (intra-valley) or the q-points connecting that valley by another of the six valleys (inter-valley).

For metals, we have found it more efficient to perform tetrahedron integration over the entire Brillouin zone (BZ). Due to the complexity of the Fermi-surface of many metals it is hard to know the relevant q-points connecting the k-points beforehand. Therefore, we have added the option to perform tetrahedron integrations over Monkhorst-Pack grids in the full Brillouin zone for the q-point sampling. Specifically, the tetrahedron integration consists of changing the sum over q-points and the delta-function to the tetrahedron interpolation scheme. Delta functions occur in the q-dependent integrals for obtaining the scattering rates[7] and in k-dependent integrals of the energy resolved transport coefficients:

$$\sigma(E) \quad = \quad \sum_{n\mathbf{k}} \sigma(n\mathbf{k})\delta(E - E_{n\mathbf{k}})\,. \tag{3}$$

Here $E_{n\mathbf{k}}$ is the bloch-state eigenvalues and the tetrahedron 'weights' are obtained for the relevant transport tensors in Eq. 2. The tetrahedron interpolation and integration drastically reduce the number of q-points needed in the full BZ for metals in a similar way to the density of states. In Fig.1c we compare the obtained resistivity with the number of q-points. Clearly the needed number of q-points is far lower with the tetrahedron integration method (approximately $8x8x8$ q-points is sufficient) as compared to the direct integration (named Gaussian and needs $> 20x20x20$ q-points). To further improve the performance we have developed a two step procedure for the k-point sampling that significantly reduce simulation time without affecting the mobility values for many materials (those that have an fairly isotropic scattering rate in momentum space). Here step one consists of taking an initial k-space with a low-sampling density and a converged q-point sampling. Typically, one will obtain a scattered selection of scattering rates that corresponds to different directions in momentum-space. We then generate an isotropic scattering rate that only depends on energy from the obtained data:

$$\frac{1}{\tau(E)} = \frac{1}{dos(E)} \sum_{n\mathbf{k}} \frac{1}{\tau_{n\mathbf{k}}} \delta(E_{n\mathbf{k}} - E) \tag{4}$$

Here we have integrated over bands n, wavevector $\mathbf{k}$, $dos(E) = \sum_{n\mathbf{k}} \delta(E_{n\mathbf{k}} - E)$ is the density of states and $\delta(E)$ is the Dirac deltafunction. In the second step, we then perform a calculation on a fine k-point grid but with the energy-dependent isotropic scattering rate. Since the scattering rate

often varies slowly with varying k-point on the Fermi-surface this is a good approximation. In this way the second step only requires an evaluation of band velocities and effective masses on the dense k-point grid while the scattering rate is reused. This two-step procedure combined with either direct integrations for semiconductors and semimetals or tetrahedron integrations for metals gives an efficient and tractable simulation tool for phonon-limited mobilities of materials. In addition, it is also possible to input a predefined scattering rate as a function of energy. This is relevant either for adding another scattering mechanism, like for instance impurity scattering, on top of the phonon scattering, or in the case where a scattering rate expression is known analytically in advance. One special case of the last situation is the limit of a constant relaxation time that has been applied previously by other simulation tools[10]. Constant relaxation time calculations are then easy and highly efficient to perform and can often give a good first estimate of thermoelectric parameters of materials with a nearly constant relaxation time.

III. Results

The supercell calculation of phonons and electron-phonon coupling from first-principles was described in detail in Ref. [7]. The simulations were performed using the ATK DFT code with the PBE-GGA functional for exchange-correlation[6]. In all cases we use the QuantumATK *medium* linear combination of atomic orbitals basis-set and corresponding pseudopotentials (SG15 medium)[11]. The real-space grid cutoff was $100\,\mathrm{Ha}$ and a Fermi-Dirac occupation of $500\,\mathrm{K}$ was used. The geometries were relaxed until all forces were smaller than $0.001\,\mathrm{eV/Å}$, and $9\times9\times9$ k-points were used in the electronic structure calculations. The bulk electron-phonon interaction and phonon dispersion were obtained from $9\times9\times9$ supercell calculations.

A. Bulk phonons

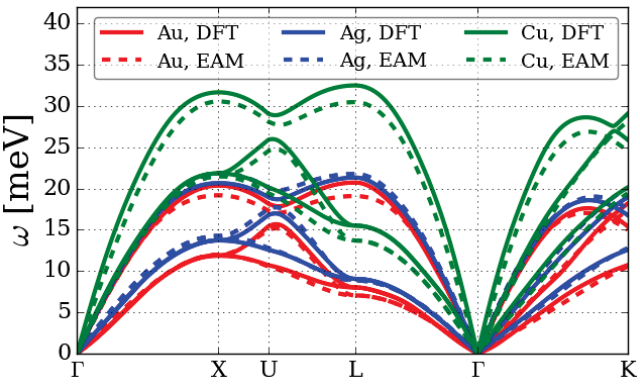

Fig. 2. Phonon dispersions of the three FCC metals Au, Ag and Cu. Dispersions obtained with DFT and the EAM force fields agree well.

In Fig. 2(c), we compare the phonon dispersion obtained with the EAM force-field and DFT. The QuantumATK DFT supercell calculation gives accurate values for the vibrational properties as exemplified by the excellent agreement between the two methods. The higher phonon frequencies of Cu can be attributed to its lower atomic mass. The bonding has a more distinct character in Au and Ag and the difference in bands are not following the difference in the atomic masses. However, overall the dispersions follow the same trends which is expected since the three FCC metals all have the same crystal symmetry. Since the chosen DFT settings and supercell repetitions give accurate values for the vibrational properties we will use these settings to evaluate the electron-phonon coupling and derived phonon-limited resistivity in the next section.

B. Bulk resistivity

We perform resistivity calculations with a sampling of $20x20x20$ q-points and tetrahedron integration. In addition, we apply the two step procedure where an k-space isotropic but energy-dependent scattering rate is generated for a low resolution k-point sampling contributing to the Fermi-surface. In the next step the full resistivity calculation is evaluated using a denser k-mesh to that correctly describes the density-of-states, carrier density, Fermi-velocity and so forth.

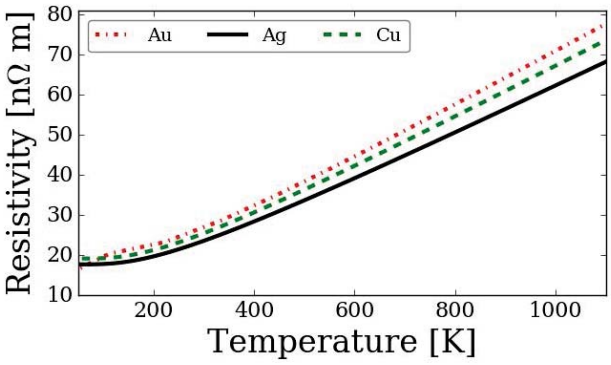

Fig. 3. Phonon-limited resistivity of the three FCC metals Au, Ag and Cu.

In Fig. 3 we show the first-principles result for the phonon limited resistivity. The resistivity increases with temperature as the phonon occupation increases and becomes linearly dependent on temperature above the Debye temperature. In agreement with experimental values we find that Au has the largest resistivity. Meanwhile Cu and Ag has almost the same resistivity but with that of Cu being slightly larger. Despite the fact that the phonon dispersions of Au and Ag are very similar the resistivity is quite different. In the minimal free electron model of metals the conductivity is given by

$$1/\rho(T) \quad = \quad \frac{1}{3}e^2 v_F^2 \tau(T) dos(\varepsilon_F)\,. \qquad (5)$$

In the three FCC metals considered the Fermi-velocity, v_F, and the density-of-states, $dos(\varepsilon_F)$, (and resulting carrier density) is almost identical and the difference in the resistivity is traced back to the variation in the scattering rate. This shows how full first-principles Boltzmann transport simulations of the

scattering rate is needed to capture the origin of the resistivity values of different metals.

Resistivity $[n\Omega\, m]$	DFT simulation	Experiment
Au, Bulk	27.0	20.5
Au, Nanowire (diameter$\approx$1 nm)	56.0	-
Ag, Bulk	23.5	14.7
Cu, Bulk	25.5	15.4

TABLE I
FIRST-PRINCIPLES RESISTIVITIES AT 300 K COMPARED WITH EXPERIMENTAL VALUES FROM REF. [12].

In table I, we present the final values for the resistivities at room temperature of bulk Au, Ag and Cu and a Au nanowire. While the resistivity of bulk Ag and Cu is slightly overestimated by the simulations, we find good agreement with experiments on bulk Au as well as the correct ranking of the individual metals which illustrates the predictive power of the simulation tools. In addition, we find that the resistivity of a 1 nm diameter Au nanowire is more than doubled as compared to that of bulk Au due to the increased electron-phonon coupling in nanowires.

IV. CONCLUSION

In summary, we have presented several extensions to the Boltzmann Transport Equation (BTE) solver implemented in QuantumATK, that enable computational efficient simulations of first-principles transport coefficients. The methods allow for calculation of linear response coefficients for an applied electric field, magnetic field or temperature gradient. We have applied the tool to calculate the phonon-limited resistivity in FCC Gold, Silver and Cobber. The scattering rates were calculated from the electron-phonon interaction from first-principles and correctly estimates the difference in the conductive properties of the three metals.

ACKNOWLEDGMENT

The authors acknowledge support from the Quantum Innovation Center (QUBIZ). CNG is sponsored by the Danish National Research Foundation, project No. DNRF103.

REFERENCES

[1] D. Josell, S. H. Brongersma, and Z. Tkei, "Size-Dependent Resistivity in Nanoscale Interconnects," *Annual Review of Materials Research*, vol. 39, no. 1, pp. 231–254, 2009. [Online]. Available: https://doi.org/10.1146/annurev-matsci-082908-145415

[2] S. L. T. Jones, A. Sanchez-Soares, J. J. Plombon, A. P. Kaushik, R. E. Nagle, J. S. Clarke, and J. C. Greer, "Electron transport properties of sub-3-nm diameter copper nanowires," *Phys. Rev. B*, vol. 92, no. 11, p. 115413, Sep. 2015. [Online]. Available: https://link.aps.org/doi/10.1103/PhysRevB.92.115413

[3] T. Gunst, T. Markussen, M. L. N. Palsgaard, K. Stokbro, and M. Brandbyge, "First-principles electron transport with phonon coupling: Large scale at low cost," *Phys. Rev. B*, vol. 96, no. 16, p. 161404, Oct. 2017. [Online]. Available: https://link.aps.org/doi/10.1103/PhysRevB.96.161404

[4] T. Gunst, K. Kaasbjerg, and M. Brandbyge, "Flexural-Phonon Scattering Induced by Electrostatic Gating in Graphene," *Phys. Rev. Lett.*, vol. 118, no. 4, p. 046601, Jan. 2017. [Online]. Available: http://link.aps.org/doi/10.1103/PhysRevLett.118.046601

[5] M. Brandbyge, J.-L. Mozos, P. Ordejón, J. Taylor, and K. Stokbro, "Density-functional method for nonequilibrium electron transport," *Phys. Rev. B*, vol. 65, no. 16, p. 165401, Mar. 2002. [Online]. Available: http://link.aps.org/doi/10.1103/PhysRevB.65.165401

[6] *Atomistix Toolkit version 2018.06, Synopsys QuantumWise A/S*.

[7] T. Gunst, T. Markussen, K. Stokbro, and M. Brandbyge, "First-principles method for electron-phonon coupling and electron mobility: Applications to two-dimensional materials," *Phys. Rev. B*, vol. 93, no. 3, p. 035414, Jan. 2016. [Online]. Available: http://link.aps.org/doi/10.1103/PhysRevB.93.035414

[8] R. Bauer, A. Schmid, P. Pavone, and D. Strauch, "Electron-phonon coupling in the metallic elements Al, Au, Na, and Nb: A first-principles study," *Phys. Rev. B*, vol. 57, no. 18, pp. 11 276–11 282, May 1998. [Online]. Available: http://link.aps.org/doi/10.1103/PhysRevB.57.11276

[9] T. Markussen, M. Palsgaard, D. Stradi, T. Gunst, M. Brandbyge, and K. Stokbro, "Electron-phonon scattering from Green's function transport combined with molecular dynamics: Applications to mobility predictions," *Phys. Rev. B*, vol. 95, no. 24, p. 245210, Jun. 2017. [Online]. Available: https://journals-aps-org.proxy.findit.dtu.dk/prb/abstract/10.1103/PhysRevB.95.245210

[10] G. K. H. Madsen and D. J. Singh, "BoltzTraP - A code for calculating band-structure dependent quantities," *Computer Physics Communications*, vol. 175, no. 1, pp. 67–71, Jul. 2006. [Online]. Available: http://www.sciencedirect.com/science/article/pii/S0010465506001305

[11] S. Smidstrup, D. Stradi, J. Wellendorff, P. A. Khomyakov, U. G. Vej-Hansen, M.-E. Lee, T. Ghosh, E. Jónsson, H. Jónsson, and K. Stokbro, "First-principles Green's-function method for surface calculations: A pseudopotential localized basis set approach," *Phys. Rev. B*, vol. 96, no. 19, p. 195309, Nov. 2017. [Online]. Available: https://link.aps.org/doi/10.1103/PhysRevB.96.195309

[12] S. Kasap, C. Koughia, and H. E. Ruda, "Electrical Conduction in Metals and Semiconductors," *Springer Handbook of Electronic and Photonic Materials*, pp. 1–1, 2017. [Online]. Available: http://link.springer.com/chapter/10.1007/978-3-319-48933-9